Catalysis Letters (2023) 153:2917–2926
https://doi.org/10.1007/s10562-022-04184-z

Photocatalytic Selective Oxidation of Toluene into Benzaldehyde on Mixed-Valence Vanadium Oxide V_6O_{13} Catalyst with Density Functional Theory

Yue-Lan Liu[1] · Yu-Feng Ding[1] · Shuang-Feng Yin[2] · Meng-Qiu Cai[1]

Received: 5 August 2022 / Accepted: 15 September 2022 / Published online: 14 November 2022

Abstract

The photocatalytic oxidation of toluene to benzaldehyde has attracted wide attention due to its mild condition, low cost and green process. In general, the traditional semiconductor photocatalytic mechanism is an oxidation–reduction reaction between photogenerated carriers and reactants. Recently, the catalyst V_6O_{13} shows the high photocatalytic activity because of the different photocatalytic mechanism from the oxidation–reduction reaction. The catalyst V_6O_{13} and aliphatic alcohol would form V_6O_{13}–alkoxide, which could be excited by visible light to effectively activate the C–H bond of α–C. However, it is unknown whether the catalyst V_6O_{13} could efficiently achieve photocatalytic oxidation of toluene and there is a similar photocatalytic mechanism for toluene by catalyst V_6O_{13}. In this work, the photocatalytic selective oxidation of toluene to benzaldehyde by V_6O_{13} catalyst is systematically investigated by density functional theory. The results show that V_6O_{13} catalyst can effectively activate toluene C(sp^3)–H bond into benzyl with the activation energy is 14.2 kcal mol^{-1}. The V_6O_{13}–toluene complex has stronger light absorption in the range from 200 to 800 nm than that of the individual V_6O_{13} clusters. Furthermore, the barrier for the dehydration of $C_6H_5CH_2OOH$ and $C_6H_5CHOHOH$ decreased from 49.0 to 35.0 kcal mol^{-1} and from 26.3 to 19.5 kcal mol^{-1}, respectively. We trace these surprising results to the novel photocatalytic mechanism that the V_6O_{13}–toluene complex could be excited by light to effectively activate the toluene C(sp^3)–H bond. Our work may provides new opportunities and challenges for photocatalytic field.

✉ Shuang-Feng Yin
sf_yin@hnu.edu.cn

✉ Meng-Qiu Cai
mqcai@hnu.edu.cn

[1] Hunan Provincial Key Laboratory of High-Energy Scale Physics and Applications, School of Physics and Electronics Science, Hunan University, Changsha 410082, People's Republic of China

[2] Advanced Catalytic Engineering Research Center of the Ministry of Education, State Key Laboratory of Chemo/Biosensing and Chemometrics, College of Chemistry and Chemical Engineering, Provincial Hunan Key Laboratory for Cost-Effective Utilization of Fossil Fuel Aimed at Reducing Carbon-Dioxide Emissions, Hunan University, Changsha 410082, Hunan, People's Republic of China

Graphical Abstract

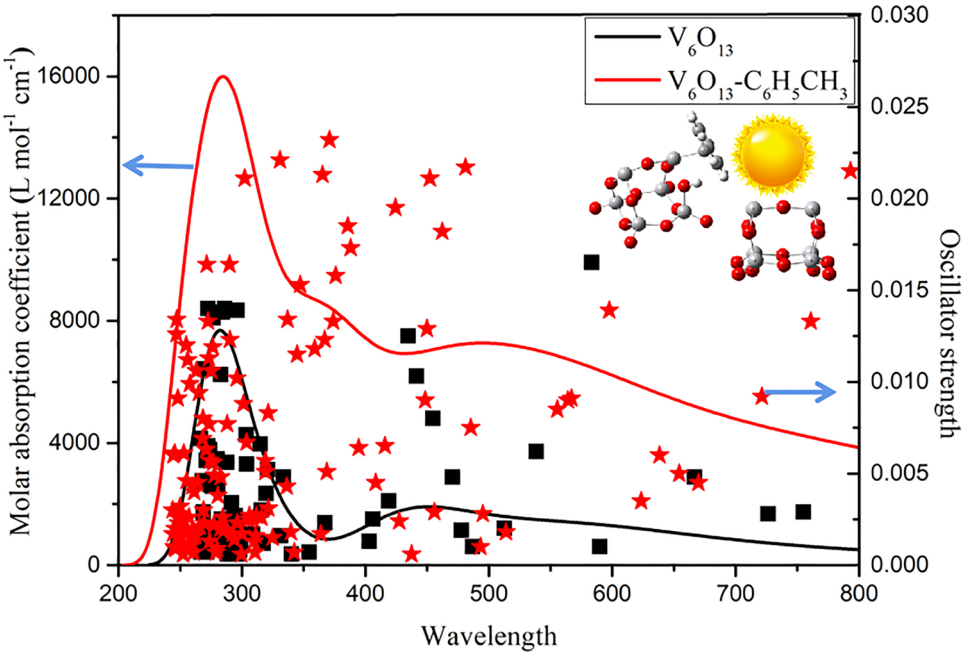

Keywords V_6O_{13} catalyst · Toluene · Selective oxidation · Photocatalysis · DFT

1 Introduction

Photocatalysis has been widely applied in various areas, such as carbon dioxide reduction [1–3], water splitting [4, 5], and pollutant degradation [6–8]. In recent years, photocatalysis has become popular in organic synthesis [9, 10], which includes selective partial oxidations, reduction reactions [11], coupling reactions [12, 13], and fuel production [14]. The synthesis of benzaldehyde (BAD) by photocatalytic oxidation of toluene has the advantages of mild reaction conditions, green reaction process, atomic economy and high target product selectivity, which has attracted high attention from researchers [15, 16]. As far as we know, the C–H bond activation is the most critical step in the photocatalytic oxidation reaction of toluene [17, 18]. Unfortunately, it is rather tricky to activate the C(sp^3)–H bonds, because of the high bond dissociation energy (85–105 kcal mol^{-1}) and chemical inertness [19]. Therefore, it is imperative to develop high-efficiency heterogeneous photocatalysts to activate the notoriously inert C–H bonds.

In general, the photocatalytic reaction process for traditional semiconductor involves three steps: (1) the semiconductor absorbs photons and is excited to produce photogenerated electron–hole pairs; (2) the separation and transfer of photogenerated electron–hole pairs; (3) the photogenerated electrons and holes participate in surface reduction and oxidation reactions, respectively [20–22]. In recent years, a variety of photocatalysts have been reported successively, which include TiO_2-based photocatalysts [18, 23], metal oxide photocatalysts [24, 25], bismuth-series semiconductor photocatalysts [26], metal sulfide [27] and non-metallic polymers [28]. Although multifarious photocatalysts have been studied, the catalytic performance of them is not ideal due to the low light absorption and the severe carrier recombination. However, Zavahir et al. [29] efficiently realized the photocatalytic selective oxidation of aliphatic alcohols to aldehydes or ketones by V_6O_{13} catalyst. The V_6O_{13} catalyst and aliphatic alcohols would form V_6O_{13}–alkoxide, which could be excited by visible light to activate the C–H bond of α–C [29]. This reaction mechanism is different from conventional semiconductor photocatalytic mechanism and common for homogeneous systems containing metal complexes [30]; also, it can be achieved in heterogeneous systems by anchoring these active metal sites on the supports, and the resulting catalysts can be termed single-atom site catalysts [31–33].

We are inspired by the work of Zavahir's group [29] to speculate that the V_6O_{13} catalyst also have the potential of toluene C(sp^3)–H activation. However, it is unknown whether the catalyst V_6O_{13} could efficiently achieve photocatalytic oxidation of toluene and there is a similar photocatalytic mechanism for toluene by catalyst V_6O_{13}.

Therefore, we present a detailed theoretical study of the photocatalytic activity and mechanism of V_6O_{13} clusters for toluene, using density functional theory (DFT) calculations to further expand the application of the catalyst V_6O_{13} in various fields. The results show that V_6O_{13} catalyst can effectively activate toluene C(sp^3)–H bond into benzyl. Moreover, The V_6O_{13}–toluene complex has excellent light absorption in the range from 200 to 800 nm, which is critical for the activation of toluene C–H bond.

2 Calculation Methods

All the calculations were performed by the density functional theory (DFT) with Gaussian 09 package [34]. The V_6O_{13} neutral clusters model is simulated [29] and the optimized structure is shown in Fig. 1. The atomic coordinates for the calculated structure of V_6O_{13} clusters is shown in Table S1. The Gibbs free energy (E) of reactants, intermediates, transition states (TS) and products in the acetonitrile solvent was calculated [35, 36]. The complete geometry optimization and vibration analysis were carried out at the B3LYP-D3(BJ)/6-31G (d) level of theory. All geometries of reactants, products, intermediates and transition states (TS) were optimized without any symmetry restriction. To improve the accuracy of the results, Grimme's DFT-D3 correction as a dispersion corrected method was taken into account. The stationary point (no imaginary frequency) and transition states (only single imaginary frequency) were identified by vibrational analyses [35, 36]. Moreover, the right transition states are confirmed by the intrinsic reaction coordinate (IRC) [50], and the SMD solvation model in acetonitrile was used to consider the influence of the solvation effect for the reaction [37–40]. The high precision single-point energy were calculated using B3LYP-D3(BJ)/def2-TZVP calculation level on the above optimized structures.

The optical absorption properties of V_6O_{13} cluster and V_6O_{13}–toluene complex were calculated using B3LYP-D3(BJ)/6-31G(d) calculation level in the time-dependent DFT (TDDFT) framework [29, 41, 42]. The light absorption spectra were plotted by the Multiwfn 3.8 software [43]. The adsorption energy E_{adp} of toluene, benzyl alcohol (BA) and benzaldehyde (BAD) was calculated as follows:

$$E_{adp} = E_{tot} - (E_{adb} + E_{pure}) \quad (1)$$

where E_{adp} is the adsorption energy. For Toluene (or BA, BAD) adsorbed on the V_6O_{13} cluster, E_{tot} is the total system energy of Toluene (or BA, BAD) adsorbed on V_6O_{13} clusters, E_{adb} is the energy of Toluene (or BA, BAD), and E_{pure} is the energy of V_6O_{13} clusters.

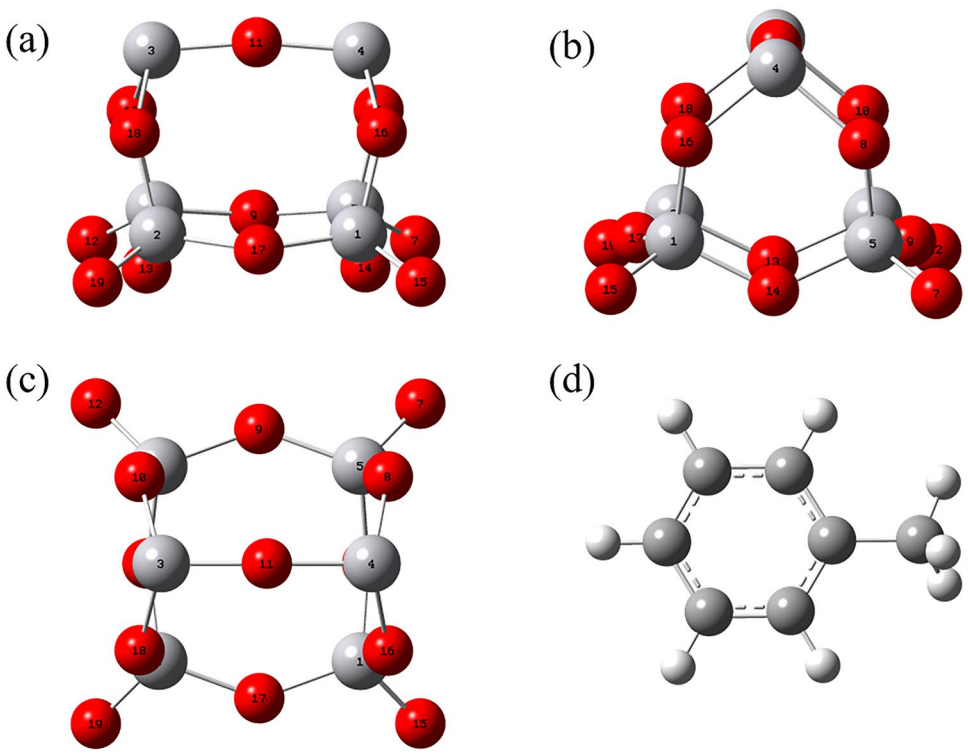

Fig. 1 The optimized structures of V_6O_{13} cluster and toluene molecular. **a** The face view of V_6O_{13} cluster; **b** the side view of V_6O_{13} cluster; **c** the top view of V_6O_{13} cluster; and **d** the optimized diagram of toluene molecular structure. In the V_6O_{13} cluster structure, red balls represent oxygen atoms, gray balls represent vanadium atoms and the number represent atomic sequence; in toluene structure, gray balls represent carbon atoms and white balls represent hydrogen atoms. Structure from Zavahir [29]

3 Results and Discussion

3.1 Activation of Toluene C(sp^3)–H Bond

As we all know, the cleavage of C(sp^3)–H bond is the first and decisive step of toluene activation. However, the dissociation energy of C(sp^3)–H bond is as high as 85–105 kcal mol^{-1} [17–19]. Hence, reducing the activation energy of C(sp^3)–H bond is the key for the reaction. Figure 2 shows the Gibbs free energy profile of toluene C(sp^3)–H bond activation by the V_6O_{13} clusters (left) and the hydroxyl radical ·OH (right). The two activation processes involve transition states TS0 (left), TS1 (right) and the transition states TS0, TS1 connect the corresponding initial and final state structures, respectively. The reaction energy barrier for TS0 (V_6O_{13} clusters activating toluene) is 14.2 kcal mol^{-1}, and the energy of the system is reduced by 2.2 kcal mol^{-1}. The activation reaction energy barrier for TS1 (·OH) is only 0.6 kcal mol^{-1}, and the system energy decreases by 30.7 kcal mol^{-1}. The results show that the sp^3 C–H bond of toluene is more likely to be dissociated by ·OH radical than V_6O_{13} catalyst, because the activation process for ·OH has a lower energy barrier and more energy is released from the system. As shown in Fig. 2, the catalysis mechanism of V_6O_{13} photocatalyst (TS0) is different from the widely studied V_2O_5 photocatalyst [29]. The V_2O_5 photocatalyst takes V^{5+} as the active center and reacts by semiconductor mechanism [48]. However, the V_6O_{13} photocatalyst adsorbs toluene molecule to form the V···C bond, Which could be excited by irritation. And the V···C bond length decreases to 2.060 Å from 2.381 Å. Then the O atom of V_6O_{13} catalyst would capture the H atom of toluene. Finally the resultant benzyl would bind with active species (O_2, $·O_2^-$, ·OOH and ·OH) and the V_6O_{13} catalyst enters the next cycle. By the above analysis, the activation mechanism of the C–H bond of V_6O_{13}–toluene complex is similar to that of the C–H bond activation of V_6O_{13}–alkoxide α-C proposed by Zavahir et al. [29]. From the energy point of view, the formation potential of V_6O_{13}–alkoxide (9.7 kcal mol^{-1}) is similar to that of V_6O_{13}–toluene complex (14.2 kcal mol^{-1}), which means that the formation of both V_6O_{13}–alkoxide and V_6O_{13}–toluene complex is easy under mild conditions. We suspect that the activation mode of C(sp^3)–H bond by V_6O_{13} catalysts is related to the property for V_6O_{13} material undergoing the insulator-to-metal transition at the temperature of – 123 °C [49]. More importantly, in the experimental part they achieved 100% alcohol conversion and excellent 3-hexanone selectivity (96%) by photocatalytic oxidation of 3-hexanol with V_6O_{13} clusters as an example [29]. Therefore, in our work, we prefer to introduce this similar mechanism into the activation of toluene C–H bond to achieve efficient toluene conversion and BAD selectivity. For the TS1 (·OH), the adsorbed ·OH in the vicinity of the V_6O_{13} photocatalyst would capture the H atom of toluene to generate benzyl and H_2O molecule. Moreover, the superoxide radical anion $·O_2^-$, the hydroperoxyl radicals ·OOH and molecular oxygen O_2 also were

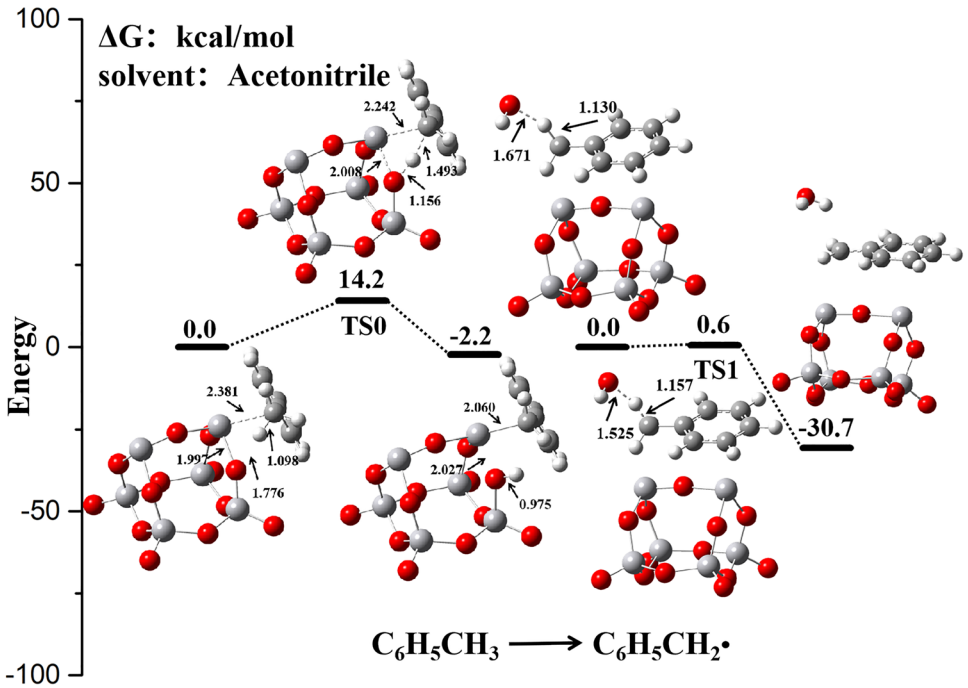

Fig. 2 Gibbs free energy profile of C–H bond activation process from toluene to benzyl radical by V_6O_{13} cluster catalyst (left) and ·OH (right) radical. Bond distances are in Å

compared. It should be pointed out that, for $^{\cdot}O_2^-$, $^{\cdot}OOH$ and O_2, the reaction energy are shown to be endothermic ($\Delta G > 0$), which means it is unlikely to take place under mild reaction condition.

3.2 UV–Vis Spectrum

In order to further explore the photocatalysis mechanism of V_6O_{13} catalyst, we also calculated the optical absorption properties of V_6O_{13} cluster and V_6O_{13}–toluene. As shown in Fig. 3, we plotted the optical absorption spectrum in the range from UV to visible light by calculating the excited states of V_6O_{13} cluster and V_6O_{13}–toluene. First, we import the calculated jump energies and oscillator intensities of each electronic excited state into Multiwfn 3.8 software [43]. Second, we enter the 11/3/2 function in Multiwfn 3.8 software in turn to output the spectral curve, and finally import the output file into Origin software for plotting. The results show that the V_6O_{13}–toluene complex has excellent light absorption both in the UV and visible region. Moreover, it is clear that the V_6O_{13}–toluene has more excited states and stronger light absorption compared to the individual V_6O_{13} cluster. It is therefore likely that visible light excites the V_6O_{13}–toluene and cleavage of the C−H bond of toluene in the light-excited state of V_6O_{13}–toluene would be much easier than that in the unexcited state. Based on the above discussions, the irradiation is an important reason for the activation of toluene, and the excellent light absorption of V_6O_{13}–toluene complex in visible region from 400 to 800 nm increases the possibility of V_6O_{13} photocatalyst application in industry.

3.3 The Possible Reaction Path of Benzyl Oxidation to BA and BAD

After conversion of toluene to benzyl, the benzyl quickly binds with active species and continues subsequent reactions, the specific oxidation path is shown in Scheme 1a. The solid line arrows in the profile represent thermodynamically favorable paths, and the red and blue numbers represent the energy barrier and the reaction Gibbs free energy (kcal mol^{-1}), respectively. We considered four active species, such as O_2, $^{\cdot}O_2^-$, $^{\cdot}OOH$ and $^{\cdot}OH$. The reaction of benzyl with the O_2, $^{\cdot}O_2^-$, $^{\cdot}OOH$ and $^{\cdot}OH$ active species is exothermic by 17.8, 21.0, 30.5, and 32.7 kcal mol^{-1}, respectively, where the reaction is a barrier-free reaction.

From the thermodynamically favorable path, the benzyl would react with O_2 and $^{\cdot}O_2^-$ to generate $C_6H_5CH_2OO^{\cdot}$ and $C_6H_5CH_2OO^-$ intermediates [44], and then bind with benzyl and proton [46, 47] to generate the TS2 ($C_6H_5CH_2OO$–$C_6H_5CH_2$) transition state and TS3 ($C_6H_5CH_2OOH$) transition state [44], respectively. The transition state TS2 generates BA and BAD through an intramolecular dissociation reaction, whereas the transition state TS3 generates BAD and H_2O molecule by a dehydration reaction. For the $^{\cdot}OOH$, the reaction rule is similar to the $^{\cdot}O_2^-$, which could generates BAD and H_2O molecule by the transition state TS3. For the $^{\cdot}OH$, it would react with benzyl to generate BA and the specific oxidation path of BA would be detailedly discussed in Sect. 3.4.

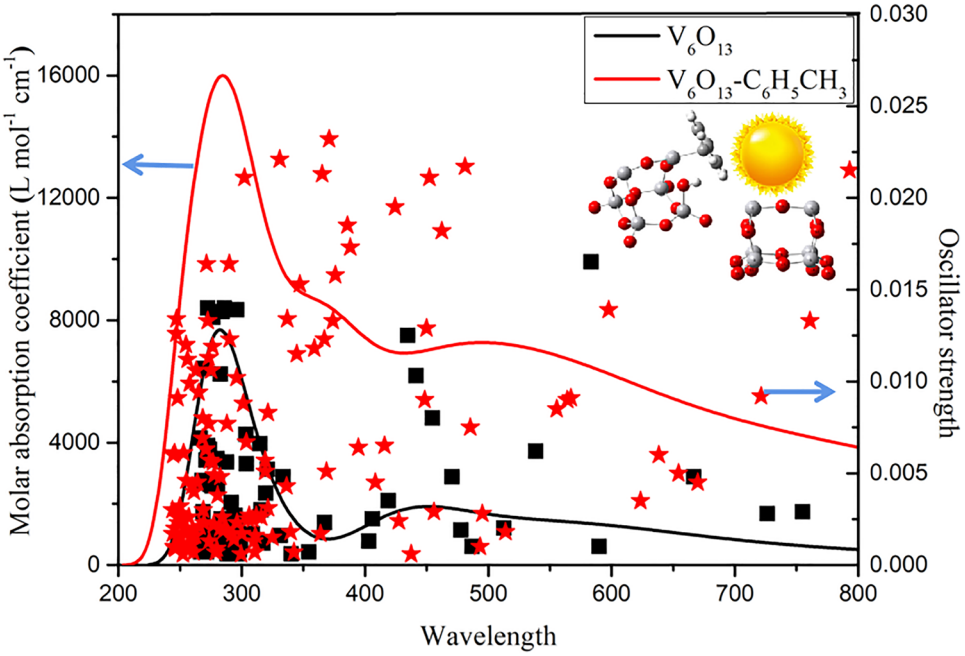

Fig. 3 The oscillator strength for the allowed excited states of individual V_6O_{13} cluster (black square) and V_6O_{13}–toluene complex (red pentagram star) in the UV–Vis light wavelength range was simulated (left axle), and the light absorption spectrum of the two structures are plotted (right axle)

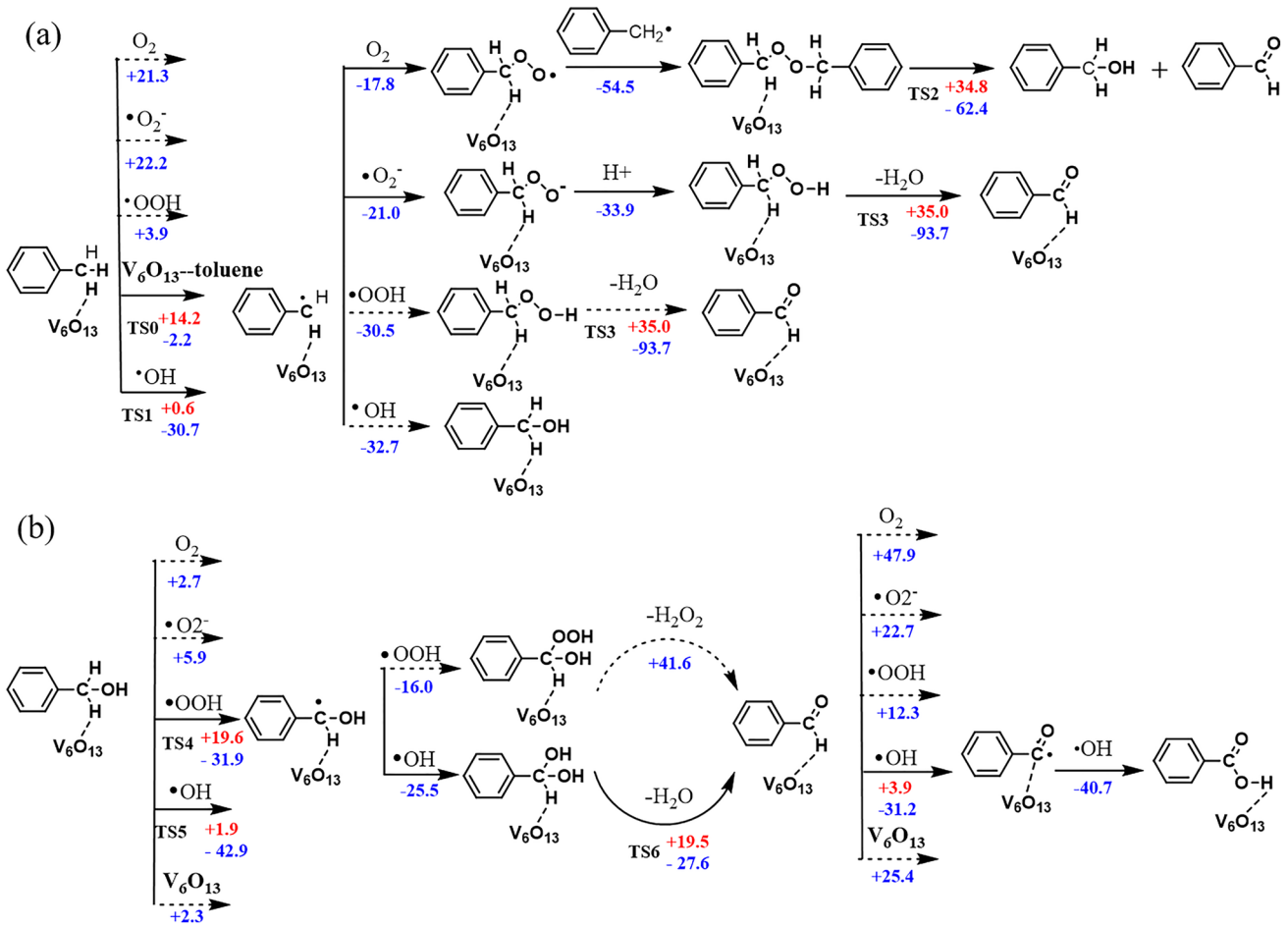

Scheme 1 **a** Reaction mechanism for toluene oxidation to BA and BAD. **b** Reaction mechanism for BA oxidation to BAD and BAD oxidation to benzoic acid. Solid lines arrows represent the thermodynamically possible paths. The red and blue numbers represent the barrier and the reaction Gibbs free energy (kcal mol^{-1}), respectively

The Gibbs free energy profile of the dissociation process of TS2 ($C_6H_5CH_2OO–CH_2C_6H_5$), as shown in Fig. 4. For the transition state TS2, the CHOO section of TS2 could form a four-element ring configuration, in which the O···O bond and the C···H bond break, and then the O atom at the far end snatches the H atom to generate BA. Subsequently, the C···O single bond becomes the C=O double bond to generate BAD, and the whole process needs to overcome the energy barrier of 34.8 kcal mol^{-1} and releases the energy of 62.4 kcal mol^{-1}. As shown in Fig. 5, the transition state TS3 ($C_6H_5CH_2OOH$) involves two possible dehydration processes, the intramolecular dehydration and the intermolecular dehydration with a water molecule participation. For the first configuration (left), the $C_6H_5CH_2OOH$ forms a four-element ring inside the molecule, and then remove a molecule of water to generate BAD. For the second configuration (right), the $C_6H_5CH_2OOH$ forms a six-element ring with a molecule of water, and eventually removes two molecules of water to form BAD. The first dehydration process requires crossing the energy barrier of 49.0 kcal mol^{-1} and releases the energy of 67.6 kcal mol^{-1}, whereas the second dehydration process only requires overcoming the energy barrier of 35.0 kcal mol^{-1} and releases more energy (93.7 kcal mol^{-1}). From the perspective of energy, the participation of water molecule promotes the reaction to a large extent. From the perspective of structure, it is likely that formation of the quaternary ring configuration causes the large molecular distortion. Hence, the participation of water molecule decreases the distortion of the molecular configuration to a certain extent, and the formation of six-element ring reduces the intramolecular tension, which is conducive to the reaction. This acceleration effect for promoting the production of BAD has been presented in experimental works. In addition, da Silva et al. [44] also calculated the energy barrier of the dehydration process for $C_6H_5CH_2OOH$ (without water molecule and catalyst participation) is 41.1 kcal mol^{-1}, which is increased by 6.1 kcal mol^{-1} than our calculation. We attribute the reduction of the barrier to the participation of V_6O_{13}

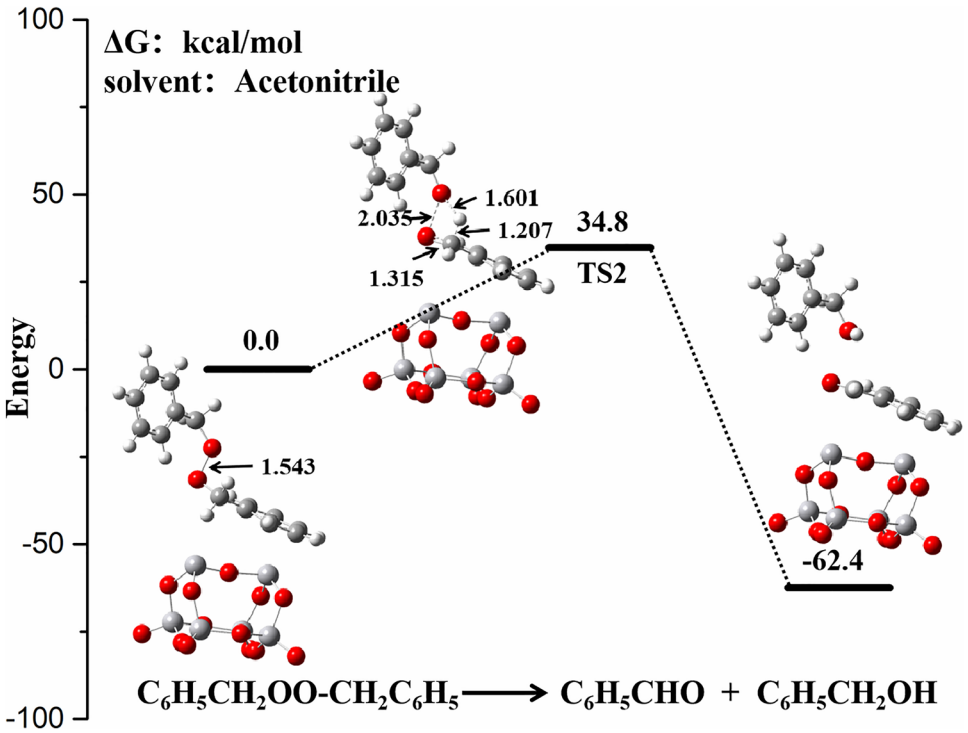

Fig. 4 Gibbs free energy profile of the dissociation process of TS2 ($C_6H_5CH_2OO–CH_2C_6H_5$). Bond distances are in Å

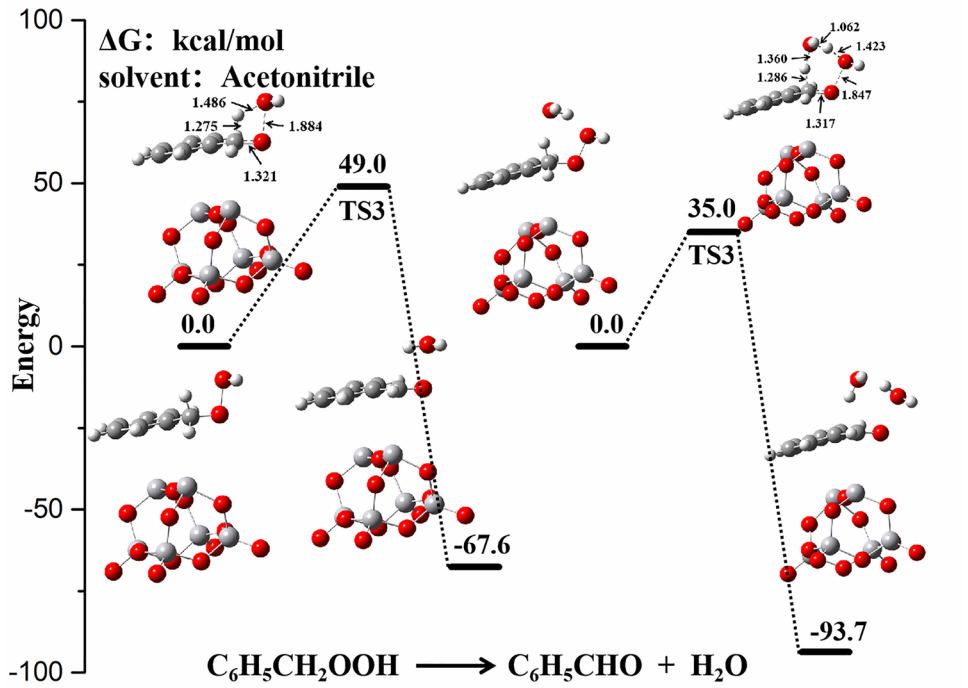

Fig. 5 Gibbs free energy profile of the $C_6H_5CH_2OOH$ dehydration process. The intramolecular dehydration is shown on the left and the intermolecular dehydration with a H_2O molecule on the right. Bond distances are in Å

catalyst and water molecule. We admit that this dehydration reaction is not easy to take place at room temperature. However, more importantly, we pay more attention to the water-induced effects in photocatalytic oxidation reactions in kinetics and thermodynamics in our study.

3.4 The Possible Reaction Path of BA Oxidation to BAD

The resultant BA would continue to be oxidized to BAD, and the specific oxidation path is shown in Scheme. 1b. The calculation results show that BA can be activated

by ·OOH radical (TS4) and ·OH radical (TS5) to form C_6H_5CHOH· intermediate. From BA to C_6H_5CHOH· by ·OOH radical, the process involves a free energy barrier of 19.6 kcal mol^{-1} and an exothermicity of 31.9 kcal mol^{-1}. From BA to C_6H_5CHOH· by ·OH radical, the free energy barrier is calculated to be 1.9 kcal mol^{-1} and it is exothermic by 42.9 kcal mol^{-1}. The specific reaction process is shown in Fig. S1. Based on the above discussions, the oxidation of BA by ·OOH and ·OH to C_6H_5CHOH· intermediate is favorable in thermodynamics and kinetics. Since the energy barrier of BA oxidation by ·OH is lower and the more system energy has been released than ·OOH, we believe that it is the main path of BA oxidation to C_6H_5CHOH· intermediate. The resulting C_6H_5CHOH· intermediate binds to the ·OH radical to generate the transition state TS6 ($C_6H_5CHOHOH$), which can remove a water molecule to generate BAD. The transition state TS6 ($C_6H_5CHOHOH$) [45] and the transition state TS3 ($C_6H_5CH_2OOH$) have the same formation mechanism, and both of them involve two possible dehydration processes, one is intramolecular dehydration, and the other is intermolecular dehydration with a water molecule participation. The formation barriers of two configurations for TS6 are 26.3 and 19.5 kcal mol^{-1} and release the energy of 2.6 and 27.6 kcal mol^{-1}, respectively, the specific dehydration process is shown in Fig. S2. The intramolecular dehydration process is through the formation of a four-element ring remove a molecule of water. The intermolecular dehydration process forms a six-element ring through $C_6H_5CHOHOH$ and a molecule of water, which finally takes off two molecules of water to generate BAD. The dehydration processes of TS3 and TS6 indicate that the presence of water molecules is a positive effect for the whole reaction. We demonstrate theoretically that water molecules and reactants could form a six-member ring to reduce the formation barrier of transition states and the molecular configuration distortion. Although water has a promoting effect on the reaction, the amount of water added is also worth studying. Some researchers found that when the water is added for more than a certain amount, the conversion rate of reactant is reduced [51–53]. We suspect there are two possible reasons. First, in the dehydration reaction, although water can act as a reactant, it is also a product. When excessive water is added, the reaction would proceed in opposite directions. The second reason is related to V_6O_{13} catalyst. Some studies have shown that the water molecule can react with V_6O_{13} catalyst, in which the V–O bond of V_6O_{13} catalyst is broken, the H_2O molecule would split into ·OH and ·H, and ·OH would connect with V atom, while ·H would connect with O atom [54]. This reaction could deactivate our catalyst, while adding excessive water will aggravate the reaction, which is harmful for the photocatalytic reaction.

3.5 The Process of BAD Oxidation to Benzoic Acid (BAC)

As shown in Scheme 1b, the BAD may be further oxidized. Similar to toluene and BA, BAD is more likely to be oxidized by the ·OH radical to produce intermediate C_6H_5CO·. As is illustrated in Fig. S3, the H atom on the aldehyde group (–CHO) of BAD is abstracted through the transition state TS7. For the process of converting BAD to intermediate C_6H_5CO·, the free energy barrier is calculated to be 3.9 kcal mol^{-1}, and the system is exothermic by 31.2 kcal mol^{-1}. The intermediate C_6H_5CO· then readily reacts with ·OH radical to form BAC, which is exothermic by 40.7 kcal mol^{-1}. Base on the above analysis, the ·OH radical has a two-sided effect for the whole reaction. On the one hand the ·OH radical can activate toluene, BA and BAD, on the other hand, the ·OH radical could cause the further oxidation of BAD to form BAC. Therefore, attention should be paid to monitoring the number of ·OH radicals in the experiment to improve the conversion rate of toluene and the selectivity of BAD.

3.6 Adsorption Energy of Toluene, BA and BAD on V_6O_{13} Clusters

In addition to the calculations of the reaction path, we also calculated the adsorption energy of toluene, BA and BAD for V_6O_{13} catalyst, respectively, − 26.6 kcal mol^{-1}, + 22.6 kcal mol^{-1} and + 4.7 kcal mol^{-1}, as shown in Fig. S4. From the perspective of energy, the adsorption energy of BA and BAD on V_6O_{13} catalyst is positive, which indicate that the adsorption processes of BA and BAD on V_6O_{13} catalyst too difficult to occur in the mild condition. That is to say, BA and BAD can not be directly activated by V_6O_{13} catalyst. In contrast, the adsorption energy of toluene on the V_6O_{13} catalyst is negative, indicating that the adsorption process is spontaneous, and toluene can be directly activated by V_6O_{13} catalyst. At the same time, it also shows that resultant BA and BAD can be quickly desorbed from the catalyst to release the active site, which is beneficial for the reaction.

4 Conclusion

In summary, our work demonstrates theoretically through DFT calculations that the catalyst V_6O_{13} can efficiently activate toluene C(sp^3)–H bonds with the activation energy is 14.2 kcal mol^{-1} and the activation mechanism is similar to the C–H bond of aliphatic alcohol by V_6O_{13} clusters, making it a good candidate material for photocatalyst. Toluene and V_6O_{13} catalyst form the V_6O_{13}–toluene complex through chemical adsorption, which can be excited by light to effectively activate the toluene C(sp^3)–H bond into benzyl. The

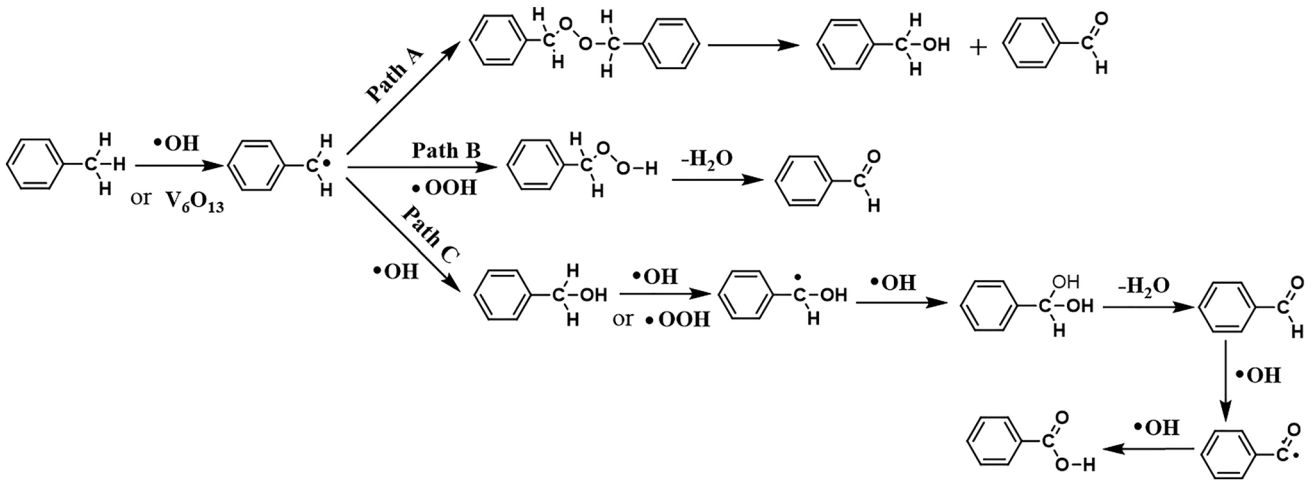

Scheme 2 The photocatalytic oxidation mechanism of toluene into BAD or BAC on V_6O_{13} cluster

V_6O_{13}–toluene complex has strong light absorption in the range from 200 to 800 nm. Therefore, for the V_6O_{13} catalyst, the excellent absorption is the key of the toluene oxidation. Moreover, we found that water can directly participate in the dehydration process to reduce the barrier of TS3 ($C_6H_5CH_2OOH$) and TS6 ($C_6H_5CHOHOH$) from 49.0 to 35.0 kcal mol^{-1} and from 26.3 to 19.5 kcal mol^{-1}, respectively. Remarkably, the ˙OH radical could rapidly oxidize BAD to BAC. Therefore, in order to get the maximum selectivity of BAD, the excess of ˙OH radical should be avoided. As shown in Scheme 2, there are three possible photocatalytic oxidation paths of toluene into BAD or BAC on V_6O_{13} catalyst. In a word, it is hoped that our study may provide new theoretical insights for the photocatalytic fields and theoretical guidance for photocatalytic selective oxidation of toluene into BAD.

Supplementary Information The online version contains supplementary material available at https://doi.org/10.1007/s10562-022-04184-z.

Acknowledgements The authors thank the Changsha Supercomputer Center for computation. This work was supported by the National Natural Science Foundation of China (Nos. 51972103, 21938002).

Declarations

Conflict of interest The authors declare no conflict of interest.

References

1. Bie C, Zhu B, Xu F, Zhang L, Yu J (2019) Adv Mater 31:1902868
2. Wang H, Raziq F, Qu Y, Qin C, Wang J, Jing L (2015) RSC Adv 5:85061–85064
3. Liang J, Li L (2017) J Mater Chem A 5:10998–11008
4. Shin SR, Park JH, Kim K-H, Choi KM, Kang JK (2016) Chem Mater 28:7725–7730
5. Mou Z, Wu Y, Sun J, Yang P, Du Y, Lu C (2014) ACS Appl Mater Interfaces 6:13798–13806
6. Tang Z-R, Zhang Y, Zhang N, Xu Y-J (2015) Nanoscale 7:7030–7034
7. Zhang LL, Xiong Z, Zhao XS (2010) ACS Nano 4:7030–7036
8. Dai C, Liu B (2020) Energy Environ Sci 13:24–52
9. Friedmann D, Hakki A, Kim H, Choi W, Bahnemann D (2016) Green Chem 18:5391–5411
10. Lang X, Chen X, Zhao J (2014) Chem Soc Rev 43:473–486
11. Habisreutinger SN, Schmidt-Mende L, Stolarczyk JK (2013) Angew Chem Int Ed 52:7372–7408
12. Lu H, Zhao J, Li L, Gong L, Zheng J, Zhang L, Wang Z, Zhang J, Zhu Z (2011) Energy Environ Sci 4:3384
13. Fagnoni M, Dondi D, Ravelli D, Albini A (2007) Chem Rev 107:2725–2756
14. Ma Y, Wang X, Jia Y, Chen X, Han H, Li C (2014) Chem Rev 114:9987–10043
15. Song L-N, Ding F, Yang Y-K, Ding D, Chen L, Au C-T, Yin S-F (2018) ACS Sustain Chem Eng 6:17044–17050
16. Lei J, Su LB, Zeng K, Chen TQ, Qiu RH, Zhou YB, Au CT, Yin S-F (2017) Chem Eng Sci 171:404–425
17. Liang Y-F, Jiao N (2017) Acc Chem Res 50:1640–1653
18. Cao X, Han T, Peng Q, Chen C, Li Y (2020) Chem Commun 56:13918–13932
19. Sterckx H, Morel B, Maes BUW (2019) Angew Chem Int Ed 58:7946–7970
20. Bie C, Yu H, Cheng B, Ho W, Fan J, Yu J (2021) Adv Mater 33:2003521
21. Meng A, Zhang L, Cheng B, Yu J (2019) Adv Mater 31:1807660
22. Hao H, Zhang L, Wang W, Zeng S (2018) Catal Sci Technol 8:1229–1250
23. Li C-J, Xu G-R, Zhang B, Gong JR (2012) Appl Catal B-Environ 115:201–208
24. Bai H, Yi W, Li J, Xi G, Li Y, Yang H, Liu J (2016) J Mater Chem A 4:1566–1571
25. Tripathy J, Lee K, Schmuki P (2014) Angew Chem-Int Edit 53:12605–12608
26. Liu Y, Chen L, Yuan Q, He J, Au C-T, Yin S-F (2016) Chem Commun 52:1274–1277
27. Zhang Y, Zhang N, Tang Z-R, Xu Y-J (2012) Chem Sci 3:2812–2822
28. Li X-H, Chen J-S, Wang X, Sun J, Antonietti M (2011) J Am Chem Soc 133:8074–8077

29. Zavahir S, Xiao Q, Sarina S, Zhao J, Bottle S, Wellard M, Jia J, Jing L, Huang Y, Blinco JP, Wu H, Zhu H-Y (2016) ACS Catal 6:3580–3588
30. Mironov OA, Bischof SM, Konnick MM, Hashiguchi BG, Ziatdinov VR, Goddard WA, Ahlquist M, Periana RA (2013) J Am Chem Soc 135:14644–14658
31. Shan J, Li M, Allard LF, Lee S, Flytzani-Stephanopoulos M (2017) Nature 551:605–608
32. Li L, Li G-D, Yan C, Mu X-Y, Pan X-L, Zou X-X, Wang K-X, Chen J-S (2011) Angew Chem Int Ed 50:8299–8303
33. Coperet C (2010) Chem Rev 110:656–680
34. Frisch GWTMJ, Schlegel HB, Scuseria GE, Robb JRCMA, Scalmani G, Barone V, Mennucci B, Petersson HNGA, Caricato M, Li X, Hratchian HP, Izmaylov JBAF, Zheng G, Sonnenberg JL, Hada M, Ehara KTM, Fukuda R, Hasegawa J, Ishida M, Nakajima T, Honda OKY, Nakai H, Vreven T, Montgomery Jr JA, Peralta FOJE, Bearpark M, Heyd JJ, Brothers E, Kudin VN SKN, Keith T, Kobayashi R, Normand J, Raghavachari ARK, Burant JC, Iyengar SS, Tomasi J, Cossi NRM, Millam JM, Klene M, Knox JE, Cross JB, Bakken CAV, Jaramillo J, Gomperts R, Stratmann RE, Yazyev AJAO, Cammi R, Pomelli C, Ochterski JW, Martin KMRL, Zakrzewski VG, Voth GA, Salvador JJDP, Dapprich S, Daniels AD, Farkas JBFO, Cioslowski JV, Fox ADJ Gaussian 09 Revision D01 Gaussian Inc Wallingford CT (2013)
35. Becke AD (1988) Phys Rev A 38:3098–3100
36. Lee C, Yang W, Parr RG (1988) Phys Rev B 37:785–789
37. Marenich AV, Cramer CJ, Truhlar DG (2009) J Phys Chem B 113:6378–6396
38. Ho J, Klamt A, Coote ML (2010) J Phys Chem A 114:13442–13444
39. Huang X, Gan HL, Peng L, Gu FL (2016) Chem J Chin U 37:297–305
40. Ribeiro RF, Marenich AV, Cramer CJ, Truhlar DG (2011) J Phys Chem B 115:14556–14562
41. van Gisbergen SJA, Snijders JG, Baerends EJ (1999) Comput Phys Commun 118:119–138
42. Adamo C, Jacquemin D (2013) Chem Soc Rev 42:845–856
43. Lu T, Chen FW (2012) J Comput Chem 33:580–592
44. da Silva G, Hamdan MR, Bozzelli JW (2009) J Chem Theory Comput 5:3185–3194
45. Zhao L, Zhang B, Xiao X, Gu FL, Zhang R-Q (2016) J Mol Catal A Chem 420:82–87
46. Kelly CP, Cramer CJ, Truhlar DG (2007) J Phys Chem B 111:408–422
47. Fifen JJ, Dhaouadi Z, Nsangou M (2014) J Phys Chem A 118:11090–11097
48. Teramura K, Ohuchi T, Shishido T, Tanaka T (2009) J Phys Chem C 113:17018–17024
49. Monfort O, Petriskova P (2021) Processes 9:214
50. Fukui K (1981) Acc Chem Res 14:363–368
51. Ma J, Yu J, Chen W, Zeng A (2016) Catal Lett 146:1600–1610
52. Yang D, Wu T, Chen C, Guo W, Liu H, Han B (2017) Green Chem 19:311–318
53. Parrino F, Bellardita M, García-López EI, Marcì G, Loddo V, Palmisano L (2018) ACS Catal 8:11191–11225
54. Xu N, Ma X, Wang M, Qian T, Liang J, Yang W, Wang Y, Hu J, Yan C (2016) Electrochim Acta 203:171–177